science.sciencemag.org/cgi/content/full/science.abg5268/DC1

Supplementary Materials for

Prevalent, protective, and convergent IgG recognition of SARS-CoV-2 non-RBD spike epitopes

William N. Voss, Yixuan J. Hou[#], Nicole V. Johnson[#], George Delidakis, Jin Eyun Kim, Kamyab Javanmardi, Andrew P. Horton, Foteini Bartzoka, Chelsea J. Paresi, Yuri Tanno, Chia-Wei Chou, Shawn A. Abbasi, Whitney Pickens, Katia George, Daniel R. Boutz, Dalton M. Towers, Jonathan R. McDaniel, Daniel Billick, Jule Goike, Lori Rowe, Dhwani Batra, Jan Pohl, Justin Lee, Shivaprakash Gangappa, Suryaprakash Sambhara, Michelle Gadush, Nianshuang Wang, Maria D. Person, Brent L. Iverson, Jimmy D. Gollihar, John Dye, Andrew Herbert, Ilya J. Finkelstein, Ralph S. Baric, Jason S. McLellan, George Georgiou, Jason J. Lavinder*, Gregory C. Ippolito*

#These authors contributed equally to this work.
*Corresponding author. Email: jlavinder@utexas.edu (J.J.L.); gci@utexas.edu (G.C.I.)

Published 4 May 2021 on *Science* First Release
DOI: 10.1126/science.abg5268

This PDF file includes:

Other Supplementary Materials for this manuscript include the following:
(available at science.sciencemag.org/cgi/content/full/science.abg5268/DC1)

Materials and Methods

Austin cohort and collection of peripheral blood

All of the SARS-CoV-2 immune plasmas used for this study were collected from non-hospitalized PCR-confirmed individuals who presented with symptomatic disease. Whole blood was collected from convalescent COVID-19 subjects while they were quarantined at home. Blood draws of Study Subjects P1 and P2 occurred at days 12 and 56 post-onset of symptoms, Subject P3 at day 11, and Subject P4 at days 19 and 45. Plasma and PBMCs were separated and collected by density gradient centrifugation using Histopaque-1077 media (Sigma-Aldrich). Informed consent was obtained for all study participants under the University of Texas at Austin IRB protocol #2020-03-0085. Details of sex and age are included in fig. S1.

Expression and purification of SARS-CoV-2 proteins

For Ig-Seq antibody proteomics, the cloning, expression, and purification of the prefusion-stabilized spike ectodomain (S-ECD "S-2P"; GenBank: MN908947) encoding residues 1–1208 and containing two proline substitutions at 986 and 987 as well as other modifications, and residues 319–591 encoding the receptor binding domain (RBD), have been previously described (*1*). For cryo-EM, spike protein was expressed by transiently transfecting plasmid encoding the HexaPro spike variant (*34*) containing substitutions S383C and D985C (*35*) with a C-terminal TwinStrep tag into FreeStyle 293-F cells (Thermo Fisher) using polyethyleneimine, with 5 μM kifunensine being added 3 hours post-transfection. The cell culture was harvested 4 days after transfection and the medium was separated from the cells by centrifugation. Supernatants were passed through a 0.22-μm filter followed by passage over StrepTactin resin (IBA). The sample was further purified by size-exclusion chromatography using a Superose 6 10/300 column (GE Healthcare) in buffer containing 2 mM Tris pH 8.0, 200 mM NaCl, and 0.02% NaN_3.

ELISA

The methods for enzyme-linked immunosorbent assay to measure titers of anti-SARS-CoV-2 IgG plasma antibodies have been previously described (*36*). For determination of mAb domain-level reactivity against recombinant spike ECD, RBD, and NTD proteins, a standard indirect ELISA was used. Costar high binding 96-well assay plates (Corning) were coated with antigens (4 μg/ml) in PBS. Antigens included in-house-produced SARS-COV-2 spike ECD (*1*) (S-ECD), SARS-COV-2 spike RBD, as well as commercially obtained SARS-COV-2 spike NTD (Sino Biological). Antigen-reactive mAbs were detected with goat anti-human IgG (Fab)-horseradish peroxidase (Sigma-Aldrich) conjugate diluted 1:5000 in PBS. After washing with PBST-0.1%, the bound antibody was detected with 3,3′,5,5′-tetramethylbenzidine soluble substrate (TMB; Millipore) using a Synergy H1 Microplate Reader (BioTek Instruments, Inc.).

V_H repertoire sequencing

PBMCs were lysed in TRIzol Reagent (Invitrogen) and total RNA was extracted using RNeasy (Qiagen). First strand cDNA was synthesized from 500 ng of mRNA using SuperScript IV (Invitrogen), and cDNA encoding the V_H regions of the IgG, IgA, and IgM repertoires was amplified with a multiplex primer set (*37*) using the FastStart High Fidelity PCR System (Roche) under the following conditions: 2 min at 95°C; four cycles of 92°C for 30 s, 50°C for 30 s, 72°C for 1 min; four cycles of 92°C for 30 s, 55°C for 30 s, 72°C for 1 min; 22 cycles of 92°C for 30 s, 63°C for 30 s, 72°C for 1 min; 72°C for 7 min; hold at 4°C, as previously described (*37*). Products were sequenced by 2×300 paired-end Illumina MiSeq.

Paired V_H:V_L repertoire sequencing

PBMCs were co-emulsified with oligo d(T)25 magnetic beads (New England Biolabs) in lysis buffer (100 mM Tris pH 7.5, 500 mM LiCl, 10 mM EDTA,1% lithium dodecyl sulfate, and 5 mM dithiothreitol) using a custom flow-focusing device as previously described [(38)]. The magnetic beads were washed, resuspended in a one-step RT-PCR solution with an overlap extension V_H and V_L primer set as previously described (*38*), emulsified using a dispersion tube (IKA), and subjected to overlap-extension RT-PCR under the following conditions: 30 min at 55°C followed by 2 min at 94°C; four cycles of 94°C for 30 s, 50°C for 30 s, 72°C for 2 min; four cycles of 94°C for 30 s, 55°C for 30 s, 72°C for 2 min; 32 cycles of 94°C for 30 s, 60°C for 30 s, 72°C for 2 min; 72°C for 7 min; hold at 4°C. Amplicons were extracted from the emulsions, further amplified using a nested PCR, and sequenced using 2×300 paired-end Illumina MiSeq.

Ig-Seq sample preparation and mass spectrometry

Total IgG was isolated from 1 ml plasma using Protein G Plus Agarose (Pierce Thermo Fisher Scientific) affinity chromatography and cleaved into $F(ab')_2$ fragments using IdeS. SARS-COV-2 Spike-specific $F(ab')_2$ was isolated by affinity chromatography using recombinant antigen (1 mg SARS-CoV-2 S-2P or RBD) coupled to 0.05 mg of dry NHS-activated agarose resin (Thermo Fisher Scientific) as follows. $F(ab')_2$ (10 mg/ml in PBS) was rotated with antigen-conjugated affinity resin for 1 hour, loaded into 0.5-ml spin columns, washed 12X with 0.4 ml of Dulbecco's PBS, and eluted with 0.5-mL fractions of 1% formic acid. IgG-containing elution fractions were concentrated to dryness in a speed-vac, resuspended in ddH_2O, combined, neutralized with 1 M Tris/3 M NaOH, and prepared for liquid chromatography–tandem mass spectrometry (LC-MS/MS) as described previously (*13*) with the modifications that (i) peptide separation using acetonitrile gradient was run for 120 min and (ii) data were collected on an Orbitrap Fusion (Thermo Fisher Scientific) operated at 120,000 resolution using HCD (higher-energy collisional dissociation) in topspeed mode with a 3 s cycle time.

Bioinformatic analysis

Raw Illumina MiSeq output sequences were trimmed according to sequence quality using Trimmomatic (*39*) and annotated using MiXCR (*40*). Sequences with ≥2 reads were clustered into clonal lineages defined by 90% CDR-H3 amino acid identity using USEARCH (*41*). LC-MS/MS search databases were prepared as previously described (*13*), using custom Python scripts (available upon request). MS searches, and MS data analyses were performed as previously described (*13*), adjusting the stringency of the elution XIC:flowthrough XIC filter to 2:1. Final diversity analyses used a lineage abundance cutoff of 0.5% of total CDR3 XIC abundance in the elution. Multiple alignment of IGHV1-24 VH genes (Fig. 3C) was performed using ClustalW at the ExPASy website (https://embnet.vital-it.ch/software/ClustalW.html) with scoring matrix equal to identity, opening and end gap penalties set to one, and ending gap and separation gap penalty = 0.05. Amino acid positions of the multiply aligned sequences (Fig. 3C and Table S4) were assigned according to the IMGT numbering system (*42*).

Antibody expression and purification

Cognate V_H and V_L antibody sequences of interest were ordered as gBlocks (Integrated DNA Technologies) and cloned into a customized pcDNA 3.4 vector containing a human IgG1 Fc region. V_H and V_L plasmids were mixed at 1:2 ratio and were transfected into Expi293F cells

(Thermo Fisher Scientific), which were cultured at 37°C and 8% CO_2 for 5 days, then neutralized and centrifuged at 1000*g* for 10 min. Antibodies was isolated from filtered supernatants using Protein G Plus Agarose (Pierce Thermo Fisher Scientific) affinity chromatography, washed with 20 column volumes of PBS, eluted with 100 mM glycine-HCl pH 2.5, and neutralized with 1 M Tris-HCl pH 8.0. The antibodies were buffer-exchanged into PBS and concentrated using 10,000 MWCO Vivaspin centrifugal spin columns (Sartorius).

Binding affinity and checkerboard competition by biolayer interferometry

Bio-Layer interferometry (BLI) assays were performed using an eight-channel Octet RED96e instrument (ForteBio). Anti-hIgG Fc Capture (AHC) Biosensors (ForteBio 18-5060) were used and the assay was performed at 25°C with shaking at 1,000 rpm. For IgG1 mAb K_D measurement, antibodies were diluted to 7.5 μg/ml and immobilized onto biosensors. The serial diluted HexaPro (*34*) (200 nM to 12.5 nM) was associated for 3 min and dissociated for 5 min. The K_D were calculated using a 1:1 binding with drifting baseline model in BIAevaluation software as described (*43*). Determination of NTD-binding epitopes (checkerboard experiment) was performed using Anti-hIgG Fc Capture (AHC) Biosensors (ForteBio Inc., 18-5060) at 25°C with shaking at 1,000 rpm. The first antibody was captured at 40 μg/ml for 10 min and blocked with 50 μg/ml of IgG isotype control for 5 min. Antigen (NTD, 100 μg/ml) was associated for 5 min and 40 μg/ml of second antibody was associated for 5 min. The ForteBio Octet Data Analysis Software 9.0 was used for all analyses.

For production of spike variants used in the BLI assays (Fig. 4E), mutations were introduced into a HexaPro mammalian cell surface display plasmid as previously described (*44*). Briefly, the spike coding region was divided into five parts and cloned into a pcDNA5-based vector along with a 3X-FLAG, a Strep Tag II epitope, an HRV 3C protease site, and a PDGFR-β transmembrane domain using a high throughput automated Golden Gate cloning pipeline. HEK293T cells were transfected with the spike display variant plasmids, incubated for 48 hours, washed with PBS, and resuspended in 3C cleavage buffer (150 mM NaCl, 50 mM Tris-HCl pH 8.0). Spike variants were cleaved from the cell surface using 3C protease (Thermo Fisher; 88946), supernatant containing the spike protein was collected by centrifugation at 16,000g for 1 min, and spike was purified through a StrepTactin resin (IBA) column followed by size-exclusion chromatography using a Superose 6 Increase 10/300 column (GE Healthcare). Anti-mouse Fc capture (AMC) Biosensors (ForteBio 18-5089) were hydrated with BLI buffer for 10 min and mouse anti-FLAG IgG was immobilized to the AMC sensor tip. Spike variants were diluted twofold with BLI buffer prior to loading onto the biosensor for binding analysis.

SARS-CoV-2 Microneutralization Assay

USAMRIID: ATCC Vero E6 cells were seeded on 96-well plates 24 hours prior to infection. MAbs were normalized, threefold serially diluted, and incubated with a pre-titrated amount of SARS-CoV-2 virus (SARS-CoV-2/MT020880.1 isolate) at 37°C for 1 hour. The virus-antibody inoculum was added to the Vero E6 monolayers and incubated for 24 hours. Cells were then formalin fixed, permeabilized, and stained with a SARS-CoV nucleocapsid-specific antibody. After counterstaining, the monolayer was imaged under immunofluorescence software analyzed to quantify the presence of the detected antigen.

UNC: SARS-CoV-2 WA1 molecular clone (GenBank accession MT461669) and nLuc virus were generated previously (*45*). ATCC Vero E6 cells were seeded at 20,000 cells per well on 96-well plates prior to infection. MAb samples were tested at starting concentrations of 30–0.1 μg/ml

and were serially diluted threefold up to eight dilution spots. Diluted mAbs were mixed with 87 PFU/well WT-nLuc virus, incubated at 37°C with 5% CO_2 for 1 hour. Following incubation, the growth medium was then removed and virus–antibody mixtures were added to the cells in duplicate. Virus-only controls were included in each plate. After a 48-hour incubation at 37°C with 5% CO_2, cells were lysed, and luciferase activity was measured using Nano-Glo Luciferase Assay System (Promega) according to the manufacturer's specifications. Neutralization titers were defined as the sample dilution at which a 50% reduction in relative light units (RLU) was observed relative to the average of the virus-only control wells.

Evaluation of mAb prophylactic efficacy in the MA10 mouse model

For the inhibition of SARS-CoV-2 in the standard laboratory BALB/c mouse model, a pathogenic mouse ACE2-adapted SARS-CoV-2 variant, MA10, was constructed previously (*23, 45*). At 12-hour before infection, twelve-month-old female BALB/c mice (n=5/group) were injected intraperitoneally with 200 μg/mouse of mAb or PBS. The mice were infected intranasally with a lethal dose (10^5 or 10^4 PFU) of the MA10 virus. Body weight of individual mice was measured daily, and all the mice were euthanized at day 4 post-infection by isoflurane overdose. The right caudal lung lobe was harvested and preserved in PBS at −80°C. Viral titers in the lung tissue were measured by plaque assay on Vero E6 cells. The UNC Chapel Hill IACUC protocol for the mouse research is 20-114.

EM sample prep and data collection

Purified spike (>98% purity by SDS PAGE) and Fab CM25 were combined at a final concentration of 0.2 mg/ml and 0.8 mg/ml respectively in buffer containing 2 mM Tris-Cl pH 8.0, 200 mM NaCl, and 0.02% NaN_3. Following a 30-min incubation on ice, 3 μL of the complex was deposited on Au-300 1.2/1.3 grids (UltrAuFoil) that had been plasma cleaned for 4 min in a Solarus 950 plasma cleaner (Gatan) with a 4:1 ratio of O2/H2. The excess liquid was blotted for 3 s with a force of −4 using a Vitrobot Mark IV (Thermo Fisher) and plunge frozen into liquid ethane. A total of 3,339 micrographs were collected from a single grid with the stage at a 30° tilt using a Titan Krios (Thermo Fisher) equipped with a K3 detector (Gatan). Movies were collected using SerialEM at 22,500X magnification with a corresponding calibrated pixel size of 1.1 $Å^2$ per pixel. A full description of the data collection parameters can be found in Table S5.

Cryogenic electron microscopy (cryo-EM)

Motion correction was performed in Warp (*46*). Micrographs were then imported into cryoSPARC v2.15.0 for CTF-estimation, particle picking, 2D classification, ab initio reconstruction, heterogenous 3D refinement and homogenous refinement (*47*). 2D classification was performed using 80 classes and an uncertainty factor of 1, followed by a second round of 2D classification using 100 classes and an uncertainty factor of 3. Selected particles were then input into an ab initio reconstruction job with three classes followed by heterogeneous refinement of those three classes. The highest quality class underwent homogeneous refinement with C3 symmetry applied. To improve the CM25–NTD interface density, C3 symmetry expansion was performed followed by particle subtraction using a mask created in UCSF ChimeraX (*48*) that encompassed two of the three CM25 Fabs and all of the spike density except for the NTD bound to the third CM25 Fab. Local refinement (cryoSPARC v3.1.0) was performed using a mask encompassing one NTD and the CM25 Fab bound to it. Local refinement was limited to 3 iterations and performed using fulcrum coordinates (x,y,z) of 235.7, 228.9, and 210.6. The local shift and

rotation searches were limited to 2 pixels and 6 degrees, respectively. To improve map quality, the focused refinement volumes were processed using the DeepEMhancer tool via COSMIC^2 science gateway (*49*). An initial model was generated by docking PDBID: 6VSB (*1*) and a Fab model based on the CM25 sequence built using SAbPred ABodyBuilder (*50*) into map density via UCSF Chimera (*51*). The model was built further and iteratively refined using a combination of Coot, Phenix, and ISOLDE (*52-54*). The full cryo-EM processing workflow and structure validation can be found in Figs. S7 and S8.

Statistics

GraphPad Prism version 9.0.0 (GraphPad Software Inc., La Jolla, CA, USA) was used to conduct statistical analyses. Non-parametric Mann–Whitney *U* tests and analysis of variance on ranks (Kruskal–Wallis *H* tests) were used to determine the statistical significance of population means between two or more groups, respectively. Statistical differences in MA10 mouse modeling were tested using a one-way ANOVA with Dunnet's multiple comparisons test, comparing every group with the mock-challenge lung titers.

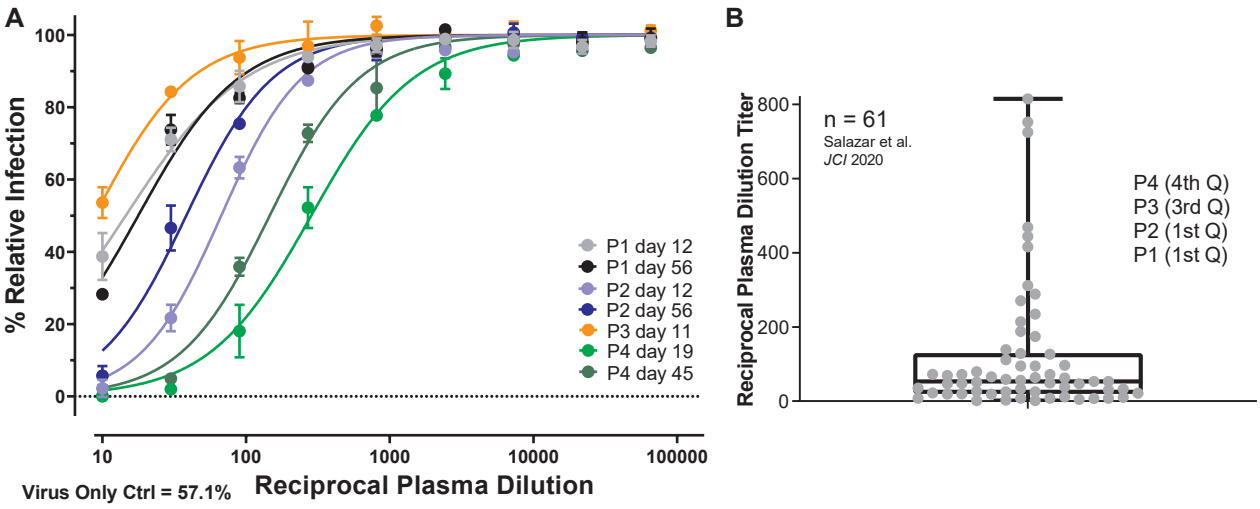

Fig. S1. Live virus neutralization titers of four COVID+ study subjects' plasma at each collection time point.
(**A**) Serial dilutions of plasma were tested in duplicate (SD error bars) for inhibition of live SARS-CoV-2 virus infection of in vitro monolayered Vero E6 cells. The percent of infected Vero E6 cells in each sample dilution was normalized relative to the virus-only (no plasma) negative control sample. (**B**) Study subjects examined in this work have a distribution of plasma neutralization titers that span from the 1st quartile (Q) to the 4th quartile as compared to a previously examined cohort of study subjects in Salazar et al. JCI 2020.

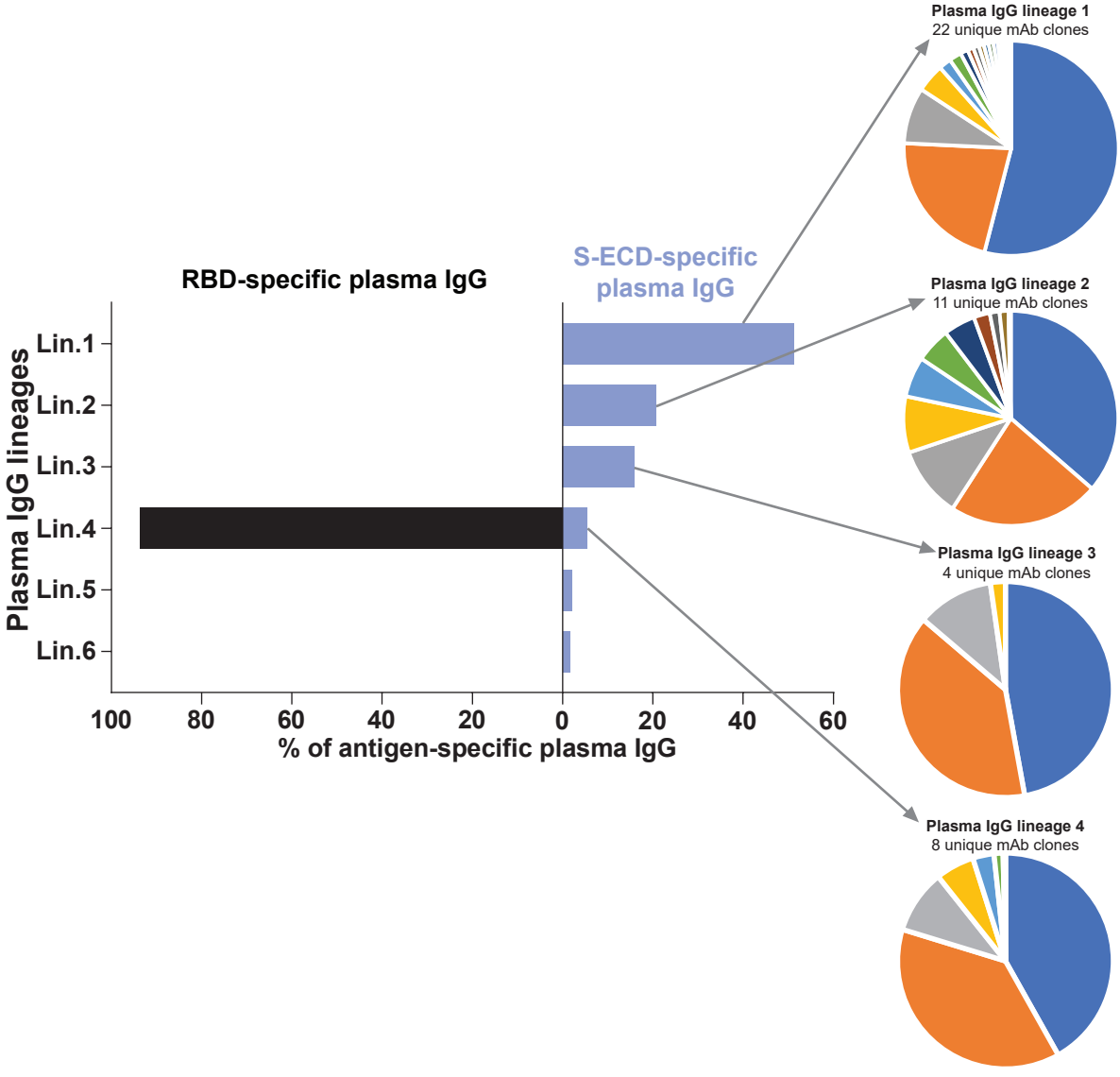

Fig. S2. Ig-seq intralineage diversification in study subject P3 at day 11.
The top four plasma IgG lineages from subject P3 demonstrate a large number of LC-MS/MS identified unique CDR-H3 clones within each lineage (45 total unique CDR-H3 clones in top four IgG lineages combined). This indicates extensive ongoing diversification within this donor at early convalescence.

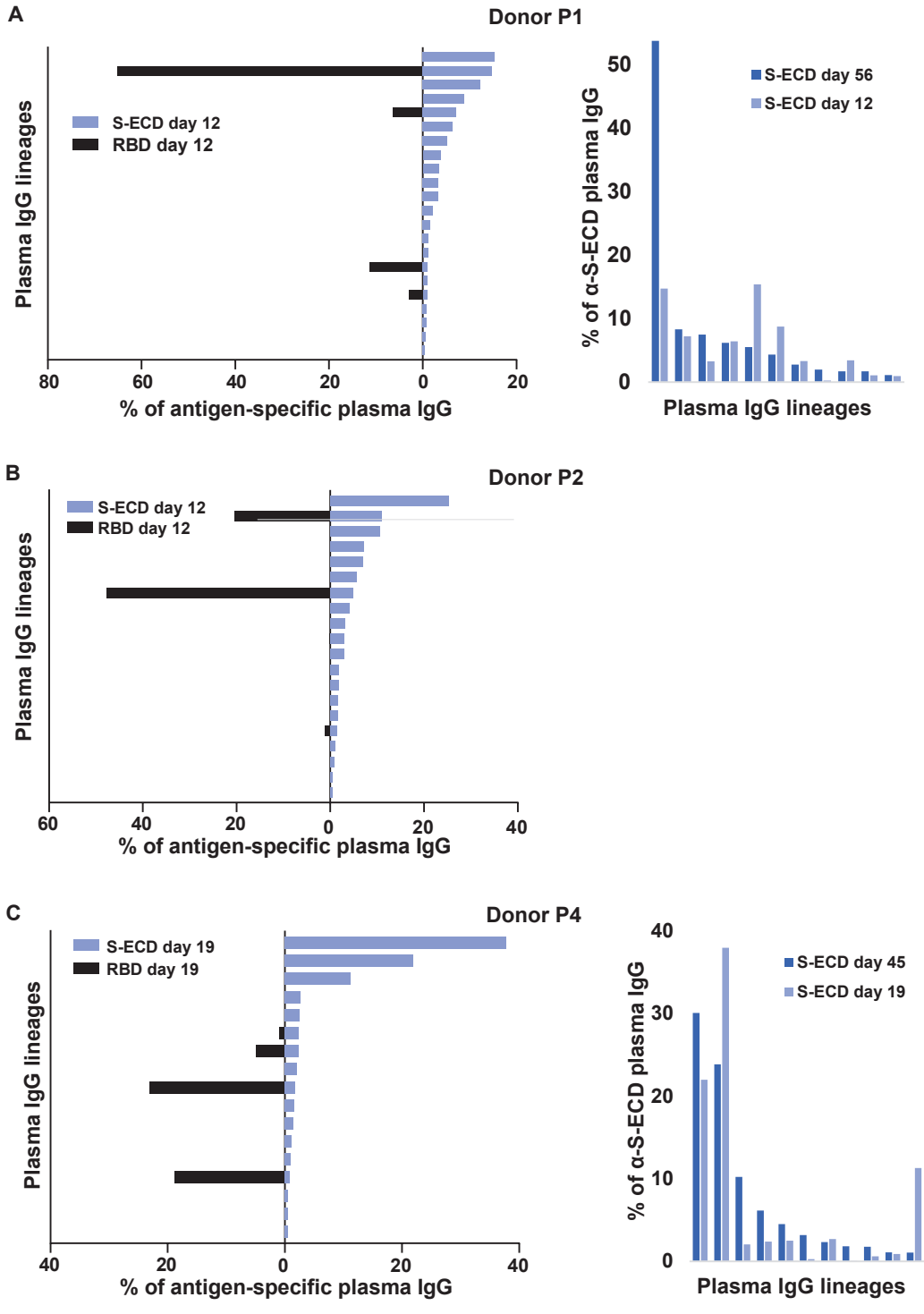

Fig. S3. Ig-seq plasma IgG lineage profiles of study subjects at early and late convalescent time points.
On the left, the first time point Ig-seq profile (days 11-19) for each subject (subject P3 found in Fig.1) shows both the SARS-CoV-2 spike ECD (S-ECD) and RBD abundance for each lineage detected at >0.5% S-ECD plasma IgG (summed lineage XIC). Similarly, on the right, the second time point data for S-ECD (days 45-56) is shown for each lineage detected at >0.5% S-ECD plasma IgG abundance (time point 2), alongside early time point S-ECD data for comparison (subject P2 found in Fig.2).

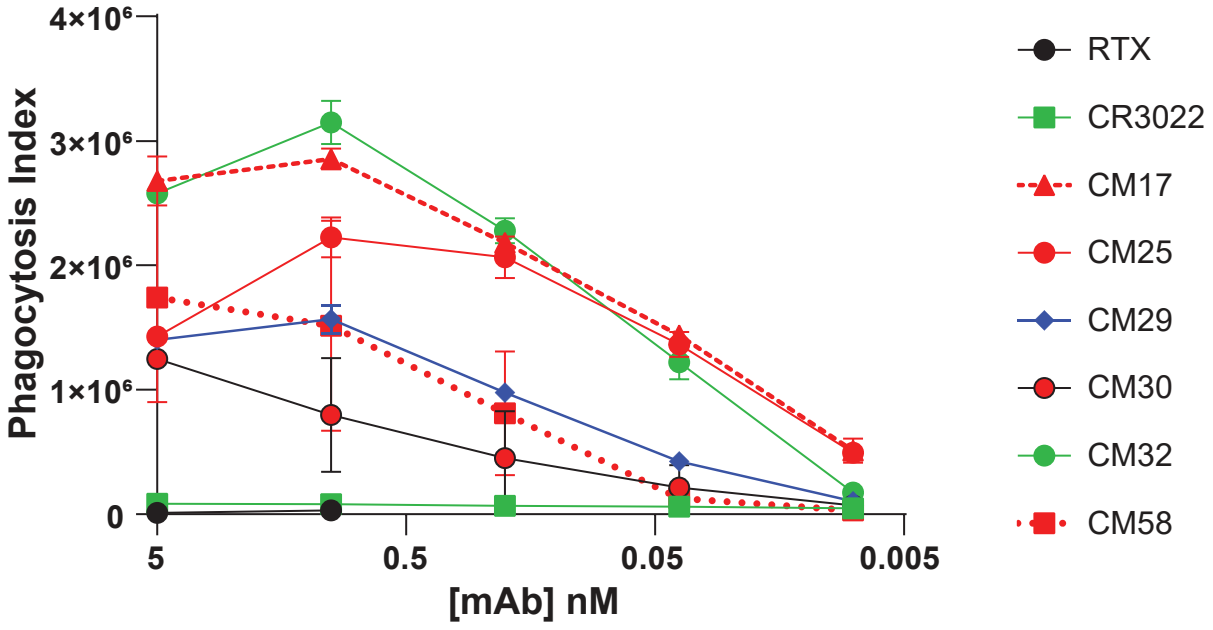

Fig. S4. ADCP ECD-bead assay using recombinant plasma IgG mAbs.
ADCP activity of recombinant plasma mAbs serially diluted on THP-1 cells in the presence of spike-conjugated, fluorescent polystyrene beads. The phagocytosis index metric represents the percent of bead-positive THP-1 cells multiplied by the average MFI of each cell to account for increased levels of bead internalization.

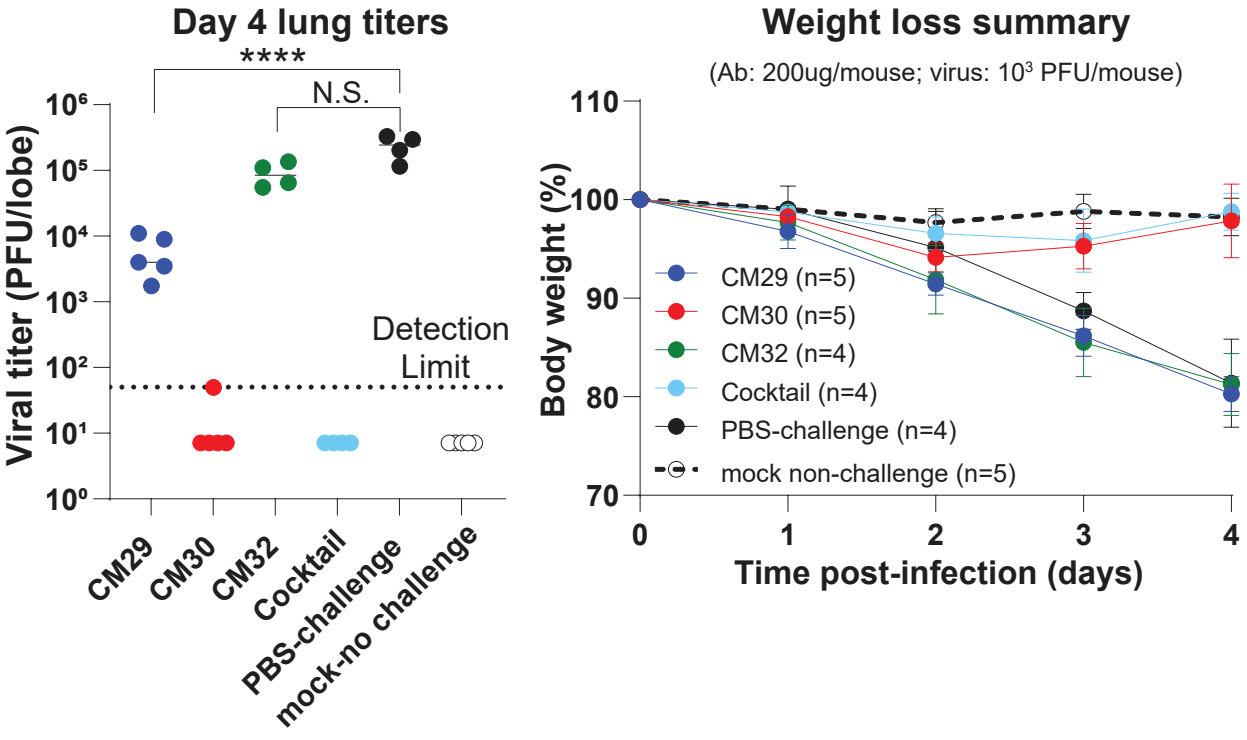

Fig. S5. In vivo protection against SARS-CoV-2 low dose viral challenge using recombinant plasma IgG mAbs. Day 4 lung viral titers and average cohort weight loss of 12-month-old BALB/C mice after intranasal challenge with 10^3 PFU (low dose) of mouse-adapted (MA10) SARS-CoV-2. A total of 200 µg mAb was administered 12 hours prior to challenge. Cocktail consisted of all four of the top donor P3 plasma IgG lineages (CM29, CM30, CM31, and CM32) in combination.

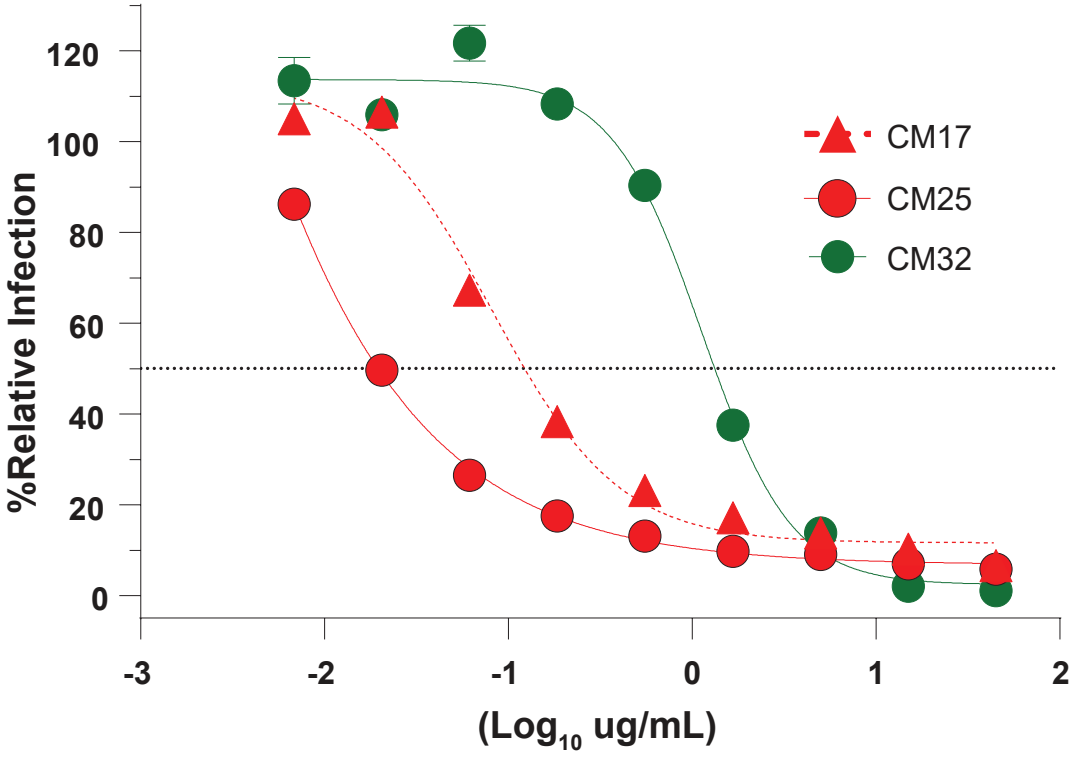

Fig. S6. Independent live virus neutralization titers of recombinant plasma IgG mAbs CM17, CM25, and CM32. In vitro live virus neutralization curves for CM17, CM25, and CM32 repeated in second independent laboratory demonstrate similar levels of inhibition (as compared to data in Figs.1D and 2C) of live SARS-CoV-2 virus infection of monolayered Vero E6 cells. The percent of infected Vero E6 cells in each sample dilution was normalized relative to the virus-only (no plasma) negative control sample.

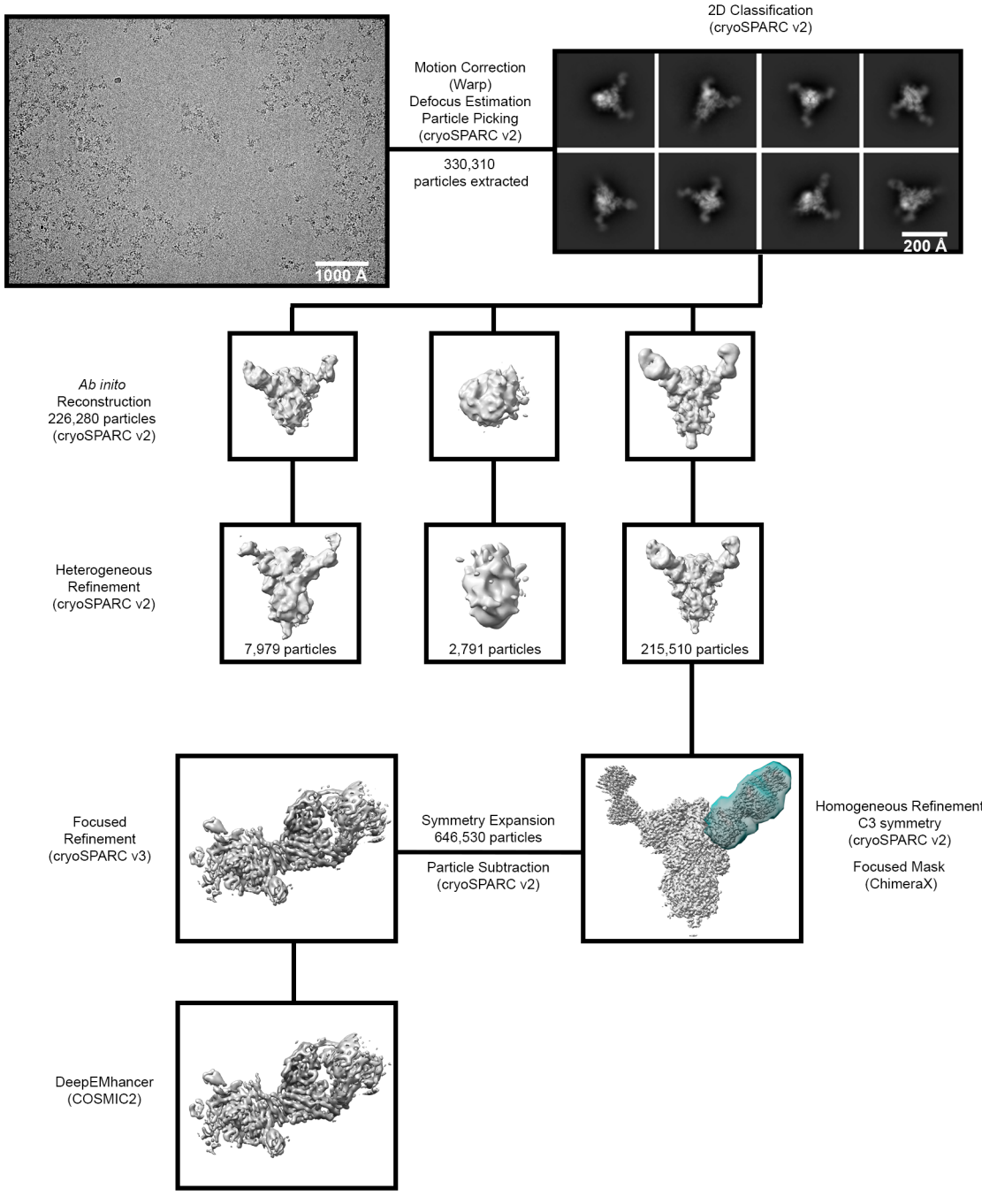

Fig. S7. Cryo-EM data processing workflow. Flowchart outlining cryo-EM data processing of SARS-CoV-2 S-ECD bound to CM25 Fab. Additional details can be found in the Methods section under "Cryogenic electron microscopy (cryo-EM)".

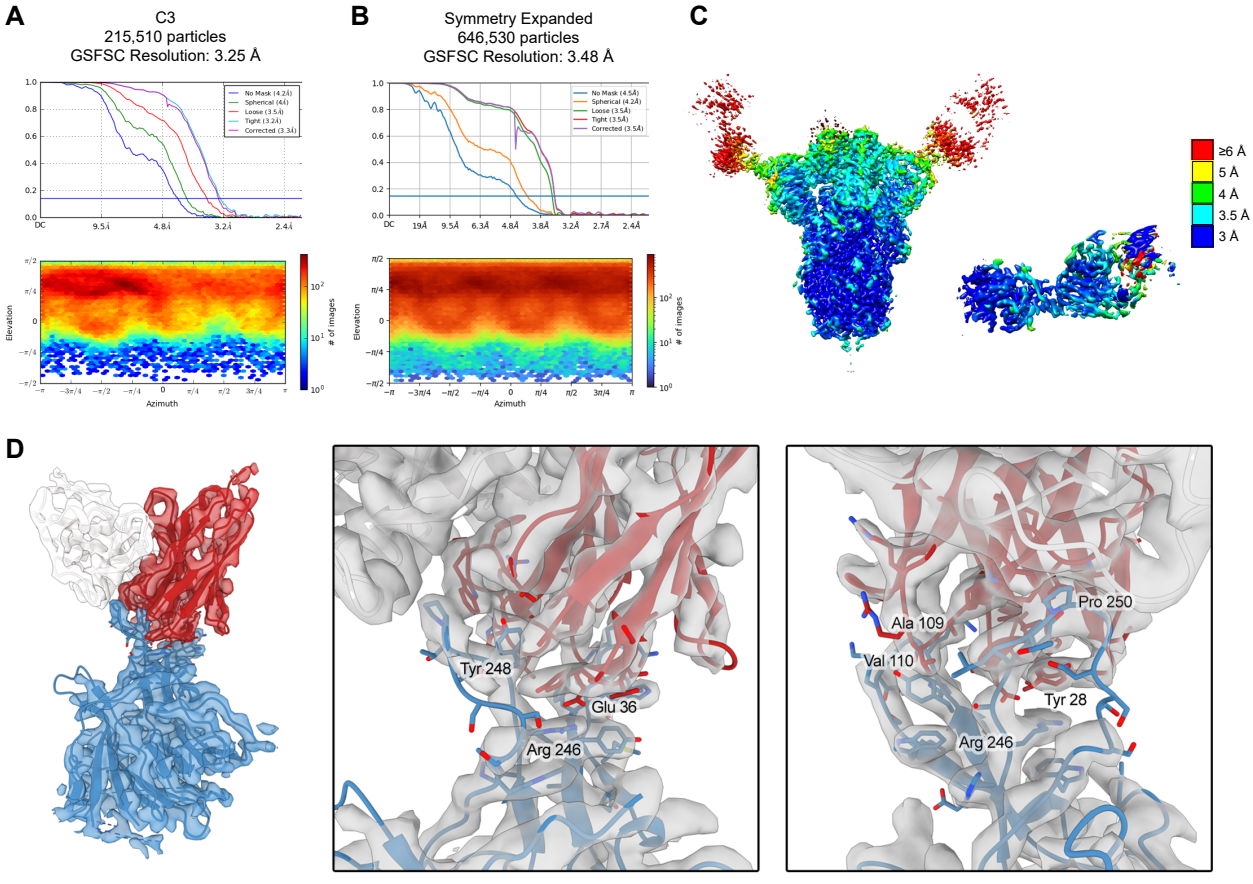

Fig. S8. Cryo-EM structure validation.
(**A)** FSC curve and viewing distribution plot for the overall S-CM25 Fab structure, generated in cryoSPARC v2.15. **(B)** FSC curve and viewing distribution plot for the focused refinement of S-NTD bound to the CM25 Fab. **(C)** Cryo-EM density of the overall S-CM25 (left) and the focused S-NTD-CM25 (right) reconstructions, colored according to local resolution. **(D)** Focused refinement density and corresponding models for the NTD (blue), CM25 Heavy chain (red), and CM25 Light chain (white). Full view of the NTD-CM25 Fab complex (left). Detailed views of the binding interface (middle, right). Oxygen atoms are colored red, nitrogen blue, and sulfurs yellow.

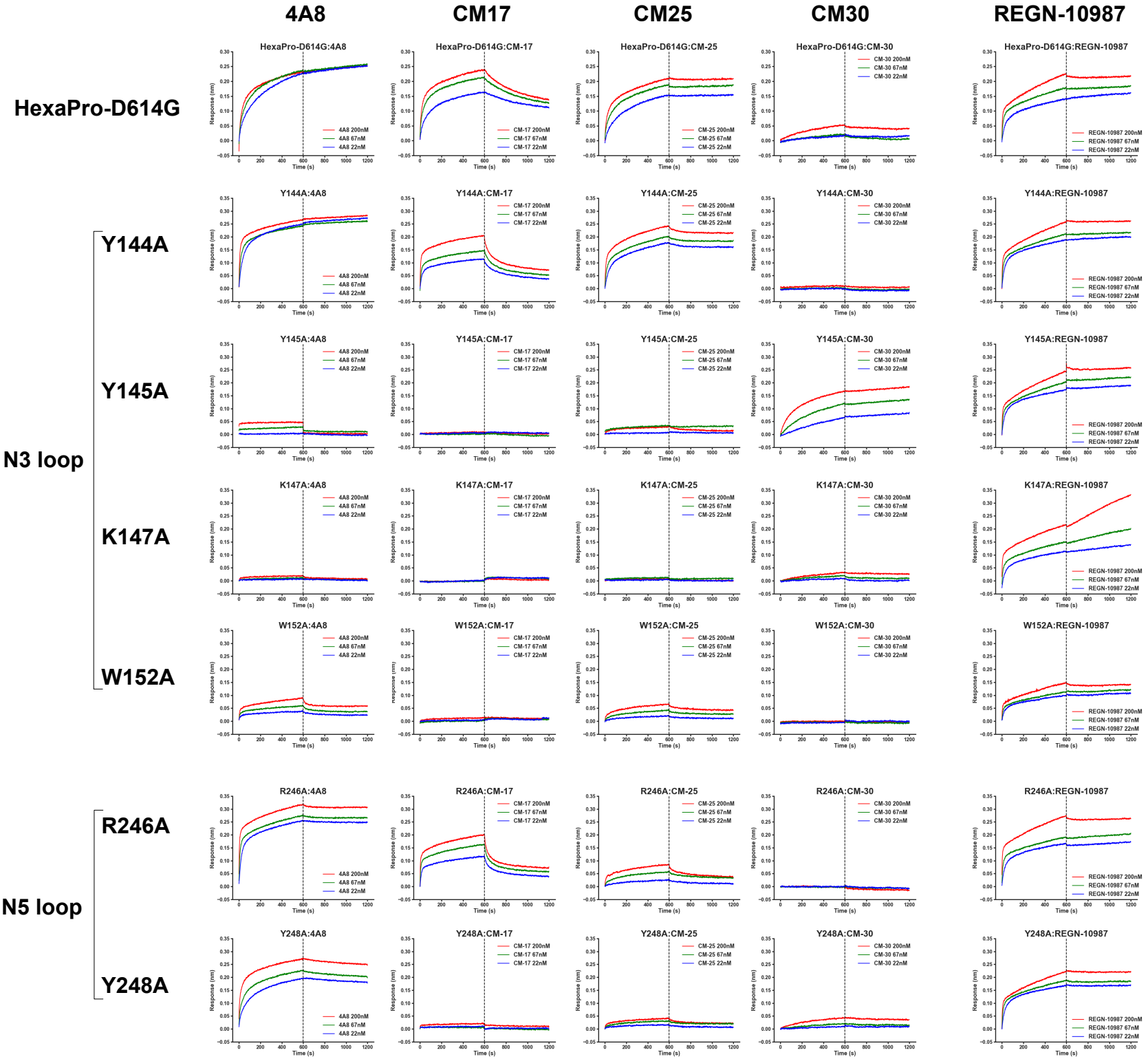

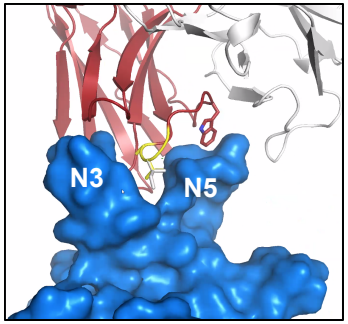

Fig. S9. Binding of anti-NTD NAbs to SARS-CoV-2 spike (S-ECD) with mutations in the N3 and N5 loops. Biolayer interferometry (BLI) sensorgrams of anti-NTD IgG and control anti-RBD IgG REGN-10987. Four residues (Y144, Y145, K147, and W152) are located in the N3 loop of the S-ECD NTD and two residues (R246 and Y248) are located in the N5 loop of the S-ECD NTD.

Table S1: Cohort Information

Subject	Age	Sex	Plasma Neut. ID50 (95% CI) (early conv.)	Plasma Neut. ID50 (95% CI) (late conv.)	mAbs	Plasma IgG Lineages (early convalescence)		
						Total	RBD	Non-RBD
P1	65	F	12.5 - 16.6	14.8 - 21.1		22	4	18
P2	35	F	60.7 - 74.5	33.6 - 43.8	CM17 CM25	20	5	15
P3	60	M	7.4 - 10.2	n.d.	CM29 CM30 CM31 CM32	6	1	5
P4	47	M	248 - 326	127 - 169	CM58	17	4	13

Table S2: Recombinant plasma mAb binding and functionality

Ab	K_D (nM)	Subject	Specificity	IC_{50} (μg/mL)	Protection
	1:1 binding		indirect ELISA	authentic virus	MA10 mouse model
CM17	9.34±0.185	P2	NTD	0.031	Full (negligible weight loss, lung viral replication)
CM25	9.44±0.055	P2	NTD	0.012	Full (negligible weight loss, lung viral replication)
CM29	6.58±0.62	P3	S2	>20	Partial (-1.5 log_{10} reduction lung titer)
CM30	0.841±0.839	P3	NTD	0.83	Full (negligible weight loss, lung viral replication)
CM31	37.7±1.65	P3	NTD	>20	None
CM32	6±0.115	P3	RBD	2.1	None
CM58	13.9±0.02	P4	NTD	0.81	Partial (-2.5 log_{10} reduction lung titer)
S309	0.015	n/a	RBD	0.075	n.d.
CR3022	34.8±13.0	n/a	RBD	>20	n.d

Table S3: Convergent NTD mAbs

Ab	IGHV	IGHD	IGHJ	CDR-H3	AA	Light Chain
CM17	1-24	3-10	4	ATAAAVRGRGTIDY	14	IGLV1-51
CM25	1-24	3-10	5	ATGPAVRRGSWFDP	14	IGLV1-51
CM58	1-24	3-10	5	ATGPVRGVIGWFDP	14	IGLV2-14
COV2-2199 (*8*)	1-24	3-10	4	ATGFAVFGRAAVPY	14	IGLV3-1
COVA2-37 (*7*)	1-24	2-2	5	ATSPAVMSVGWVDP	14	IGLV1-40
4-A8 (*4*)	1-24	6-19	6	ATSTAVAGTPDLFDYYYGMDV	21	IGKV2-24
1-68 (*5*)	1-24	6-19	6	ATGWAVAGSSDVWYYYYGMDV	21	IGLV2-18
1-87 (*5*)	1-24	6-19	6	ATGIAVIGPPPSTYYYYGMDV	21	IGLV2-14

Table S4: mAb–NTD interface analysis

	4A8			CM25				NTD (4A8)			NTD (CM25)	
	ASA(Å^2)	BSA(Å^2)		ASA(Å^2)	BSA(Å^2)			ASA(Å^2)	BSA(Å^2)		ASA(Å^2)	BSA(Å^2)
GLY27	63	10		79	15		TYR144	57	**32**		94	26
TYR28	80	**58**		103	**80**		TYR145	85	**81**		103	**75**
THR29	53	25	CDR-H1	66	14		HIS146	71	25		75	22
LEU30	4	3		25	11		LYS147	156	**147**	N3 Loop	172	**134**
THR35	106	**80**		112	**80**		ASN148	91	19		120	24
GLU36	79	**79**		89	**80**		ASN149	116	0		83	0
LEU37	13	**12**		31	**29**		LYS150	155	**69**		154	14
							SER151	49	2		24	0
PHE56	55	**37**		62	**40**		TRP152	127	**85**		148	5
ASP57	46	0		23	0							
PRO58	25	**13**	CDR-H2	37	3		HIS245	79	36		0	0
GLU59	80	8		81	0		ARG246	85	**72**		85	**62**
ASP62	127	11		100	4		SER247	46	12		64	16
GLY63	37	**24**		53	**30**		TYR248	122	**107**		170	**150**
							LEU249	182	**90**		153	**54**
GLU80	78	10		0	0		THR250	93	18	N5 Loop	77	5
							PRO251	190	0		125	32
THR108	48	**33**		38	**25**	PRO108	GLY252	0	0		82	0
ALA109	26	**24**		32	**22**	ALA109	ASP253	0	0		66	1
VAL110	67	**65**		133	**90**	VAL110	SER254	0	0		65	0
ALA111	39	**23**		139	9	ARG111	SER255	0	0		89	29
GLY111.1	73	**62**		137	0	ARG112.1	SER256	125	6		0	0
THR111.2	74	30		49	0	GLY112	GLY257	30	18		0	0
PRO111.3	131	**79**		113	0	SER113						
ASP111.4	119	0	CDR-H3	153	**91**	TRP114						
LEU112.4	124	0		98	1	PHE115						
PHE112.3	148	39		24	**18**	ASP116						
ASP112.2	89	0		73	2	PRO117						
TYR112.1	105	30										
TYR112	83	19										
TYR113	137	0										
GLY114	30	0										
MET115	62	0										
ASP116	72	11										

* bold indicates residues >50% buried surface area (BSA)

Table S5

EM data collection	
Microscope	FEI Titan Krios
Voltage (kV)	300
Detector	Gatan K3
Magnification (nominal)	22,500
Pixel size (Å/pix)	1.1
Exposure rate (e^-/pix/sec)	8
Frames per exposure	80
Exposure (e^-/Å^2)	80
Defocus range (μm)	1.5-3.0
Tilt angle (°)	30
Micrographs collected	3,339
Micrographs used	1,074
Particles extracted (total)	330,310
Automation software	SerialEM
Sample	SARS-CoV-2 S + CM25 Fab

3D reconstruction statistics	Overall	NTD-CM25 subcomplex
Particles	215,510	646,530 (symmetry expanded)
Symmetry	C3	C1
Map sharpening B-factor	-174.5	-165.1
Unmasked resolution at 0.5 FSC (Å)	6.65	4.16
Masked resolution at 0.5 FSC (Å)	4.22	3.78
Unmasked resolution at 0.143 FSC (Å)	3.64	3.52
Masked resolution at 0.143 FSC (Å)	3.25	3.48

Model refinement and validation statistics	
Refinement package	Phenix
Refinement tool	Real-space refinement
Refinement strategies	min global, local_grid_search, adp, ss restraints, rotamer restraints, ramachandran restraints
Composition	
Amino acids	453
RMSD bonds (Å)	0.006
RMSD angles (°)	0.96
Average B-factors	
Amino acids	93.27
Ramachandran	
Favored (%)	93.23
Allowed (%)	6.77

Outliers (%)	0
Rotamer outliers (%)	0
Clash score	11.44
C-beta outliers (%)	0
CaBLAM outliers (%)	2.54
CC (mask)	0.80
MolProbity score	2.01
EMRinger score	2.61

References and Notes

1. D. Wrapp, N. Wang, K. S. Corbett, J. A. Goldsmith, C.-L. Hsieh, O. Abiona, B. S. Graham, J. S. McLellan, Cryo-EM structure of the 2019-nCoV spike in the prefusion conformation. *Science* **367**, 1260–1263 (2020). doi:10.1126/science.abb2507 Medline

2. A. C. Walls, Y.-J. Park, M. A. Tortorici, A. Wall, A. T. McGuire, D. Veesler, Structure, Function, and Antigenicity of the SARS-CoV-2 Spike Glycoprotein. *Cell* **181**, 281–292.e6 (2020). doi:10.1016/j.cell.2020.02.058 Medline

3. K. McMahan, J. Yu, N. B. Mercado, C. Loos, L. H. Tostanoski, A. Chandrashekar, J. Liu, L. Peter, C. Atyeo, A. Zhu, E. A. Bondzie, G. Dagotto, M. S. Gebre, C. Jacob-Dolan, Z. Li, F. Nampanya, S. Patel, L. Pessaint, A. Van Ry, K. Blade, J. Yalley-Ogunro, M. Cabus, R. Brown, A. Cook, E. Teow, H. Andersen, M. G. Lewis, D. A. Lauffenburger, G. Alter, D. H. Barouch, Correlates of protection against SARS-CoV-2 in rhesus macaques. *Nature* **590**, 630–634 (2021). doi:10.1038/s41586-020-03041-6 Medline

4. X. Chi, R. Yan, J. Zhang, G. Zhang, Y. Zhang, M. Hao, Z. Zhang, P. Fan, Y. Dong, Y. Yang, Z. Chen, Y. Guo, J. Zhang, Y. Li, X. Song, Y. Chen, L. Xia, L. Fu, L. Hou, J. Xu, C. Yu, J. Li, Q. Zhou, W. Chen, A neutralizing human antibody binds to the N-terminal domain of the Spike protein of SARS-CoV-2. *Science* **369**, 650–655 (2020). doi:10.1126/science.abc6952 Medline

5. L. Liu, P. Wang, M. S. Nair, J. Yu, M. Rapp, Q. Wang, Y. Luo, J. F.-W. Chan, V. Sahi, A. Figueroa, X. V. Guo, G. Cerutti, J. Bimela, J. Gorman, T. Zhou, Z. Chen, K.-Y. Yuen, P. D. Kwong, J. G. Sodroski, M. T. Yin, Z. Sheng, Y. Huang, L. Shapiro, D. D. Ho, Potent neutralizing antibodies against multiple epitopes on SARS-CoV-2 spike. *Nature* **584**, 450–456 (2020). doi:10.1038/s41586-020-2571-7 Medline

6. D. F. Robbiani, C. Gaebler, F. Muecksch, J. C. C. Lorenzi, Z. Wang, A. Cho, M. Agudelo, C. O. Barnes, A. Gazumyan, S. Finkin, T. Hägglöf, T. Y. Oliveira, C. Viant, A. Hurley, H.-H. Hoffmann, K. G. Millard, R. G. Kost, M. Cipolla, K. Gordon, F. Bianchini, S. T. Chen, V. Ramos, R. Patel, J. Dizon, I. Shimeliovich, P. Mendoza, H. Hartweger, L. Nogueira, M. Pack, J. Horowitz, F. Schmidt, Y. Weisblum, E. Michailidis, A. W. Ashbrook, E. Waltari, J. E. Pak, K. E. Huey-Tubman, N. Koranda, P. R. Hoffman, A. P. West Jr., C. M. Rice, T. Hatziioannou, P. J. Bjorkman, P. D. Bieniasz, M. Caskey, M. C. Nussenzweig, Convergent antibody responses to SARS-CoV-2 in convalescent individuals. *Nature* **584**, 437–442 (2020). doi:10.1038/s41586-020-2456-9 Medline

7. P. J. M. Brouwer, T. G. Caniels, K. van der Straten, J. L. Snitselaar, Y. Aldon, S. Bangaru, J. L. Torres, N. M. A. Okba, M. Claireaux, G. Kerster, A. E. H. Bentlage, M. M. van Haaren, D. Guerra, J. A. Burger, E. E. Schermer, K. D. Verheul, N. van der Velde, A. van der Kooi, J. van Schooten, M. J. van Breemen, T. P. L. Bijl, K. Sliepen, A. Aartse, R. Derking, I. Bontjer, N. A. Kootstra, W. J. Wiersinga, G. Vidarsson, B. L. Haagmans, A. B. Ward, G. J. de Bree, R. W. Sanders, M. J. van Gils, Potent neutralizing antibodies from COVID-19 patients define multiple targets of vulnerability. *Science* **369**, 643–650 (2020). doi:10.1126/science.abc5902 Medline

8. S. J. Zost, P. Gilchuk, J. B. Case, E. Binshtein, R. E. Chen, J. P. Nkolola, A. Schäfer, J. X. Reidy, A. Trivette, R. S. Nargi, R. E. Sutton, N. Suryadevara, D. R. Martinez, L. E.

Williamson, E. C. Chen, T. Jones, S. Day, L. Myers, A. O. Hassan, N. M. Kafai, E. S. Winkler, J. M. Fox, S. Shrihari, B. K. Mueller, J. Meiler, A. Chandrashekar, N. B. Mercado, J. J. Steinhardt, K. Ren, Y.-M. Loo, N. L. Kallewaard, B. T. McCune, S. P. Keeler, M. J. Holtzman, D. H. Barouch, L. E. Gralinski, R. S. Baric, L. B. Thackray, M. S. Diamond, R. H. Carnahan, J. E. Crowe Jr., Potently neutralizing and protective human antibodies against SARS-CoV-2. *Nature* **584**, 443–449 (2020). doi:10.1038/s41586-020-2548-6 Medline

9. A. Z. Wec, D. Wrapp, A. S. Herbert, D. P. Maurer, D. Haslwanter, M. Sakharkar, R. K. Jangra, M. E. Dieterle, A. Lilov, D. Huang, L. V. Tse, N. V. Johnson, C.-L. Hsieh, N. Wang, J. H. Nett, E. Champney, I. Burnina, M. Brown, S. Lin, M. Sinclair, C. Johnson, S. Pudi, R. Bortz 3rd, A. S. Wirchnianski, E. Laudermilch, C. Florez, J. M. Fels, C. M. O'Brien, B. S. Graham, D. Nemazee, D. R. Burton, R. S. Baric, J. E. Voss, K. Chandran, J. M. Dye, J. S. McLellan, L. M. Walker, Broad neutralization of SARS-related viruses by human monoclonal antibodies. *Science* **369**, 731–736 (2020). doi:10.1126/science.abc7424 Medline

10. T. J. Ripperger, J. L. Uhrlaub, M. Watanabe, R. Wong, Y. Castaneda, H. A. Pizzato, M. R. Thompson, C. Bradshaw, C. C. Weinkauf, C. Bime, H. L. Erickson, K. Knox, B. Bixby, S. Parthasarathy, S. Chaudhary, B. Natt, E. Cristan, T. El Aini, F. Rischard, J. Campion, M. Chopra, M. Insel, A. Sam, J. L. Knepler, A. P. Capaldi, C. M. Spier, M. D. Dake, T. Edwards, M. E. Kaplan, S. J. Scott, C. Hypes, J. Mosier, D. T. Harris, B. J. LaFleur, R. Sprissler, J. Nikolich-Žugich, D. Bhattacharya, Orthogonal SARS-CoV-2 Serological Assays Enable Surveillance of Low-Prevalence Communities and Reveal Durable Humoral Immunity. *Immunity* **53**, 925–933.e4 (2020). doi:10.1016/j.immuni.2020.10.004 Medline

11. J. A. Juno, H.-X. Tan, W. S. Lee, A. Reynaldi, H. G. Kelly, K. Wragg, R. Esterbauer, H. E. Kent, C. J. Batten, F. L. Mordant, N. A. Gherardin, P. Pymm, M. H. Dietrich, N. E. Scott, W.-H. Tham, D. I. Godfrey, K. Subbarao, M. P. Davenport, S. J. Kent, A. K. Wheatley, Humoral and circulating follicular helper T cell responses in recovered patients with COVID-19. *Nat. Med.* **26**, 1428–1434 (2020). doi:10.1038/s41591-020-0995-0 Medline

12. Y. Weisblum, F. Schmidt, F. Zhang, J. DaSilva, D. Poston, J. C. C. Lorenzi, F. Muecksch, M. Rutkowska, H.-H. Hoffmann, E. Michailidis, C. Gaebler, M. Agudelo, A. Cho, Z. Wang, A. Gazumyan, M. Cipolla, L. Luchsinger, C. D. Hillyer, M. Caskey, D. F. Robbiani, C. M. Rice, M. C. Nussenzweig, T. Hatziioannou, P. D. Bieniasz, Escape from neutralizing antibodies by SARS-CoV-2 spike protein variants. *eLife* **9**, e61312 (2020). doi:10.7554/eLife.61312 Medline

13. J. J. Lavinder, Y. Wine, C. Giesecke, G. C. Ippolito, A. P. Horton, O. I. Lungu, K. H. Hoi, B. J. DeKosky, E. M. Murrin, M. M. Wirth, A. D. Ellington, T. Dörner, E. M. Marcotte, D. R. Boutz, G. Georgiou, Identification and characterization of the constituent human serum antibodies elicited by vaccination. *Proc. Natl. Acad. Sci. U.S.A.* **111**, 2259–2264 (2014). doi:10.1073/pnas.1317793111 Medline

14. J. J. Lavinder, A. P. Horton, G. Georgiou, G. C. Ippolito, Next-generation sequencing and protein mass spectrometry for the comprehensive analysis of human cellular and serum

antibody repertoires. *Curr. Opin. Chem. Biol.* **24**, 112–120 (2015). doi:10.1016/j.cbpa.2014.11.007 Medline

15. W. E. Purtha, T. F. Tedder, S. Johnson, D. Bhattacharya, M. S. Diamond, Memory B cells, but not long-lived plasma cells, possess antigen specificities for viral escape mutants. *J. Exp. Med.* **208**, 2599–2606 (2011). doi:10.1084/jem.20110740 Medline

16. K. G. Smith, A. Light, G. J. Nossal, D. M. Tarlinton, The extent of affinity maturation differs between the memory and antibody-forming cell compartments in the primary immune response. *EMBO J.* **16**, 2996–3006 (1997). doi:10.1093/emboj/16.11.2996 Medline

17. C. O. Barnes, A. P. West Jr., K. E. Huey-Tubman, M. A. G. Hoffmann, N. G. Sharaf, P. R. Hoffman, N. Koranda, H. B. Gristick, C. Gaebler, F. Muecksch, J. C. C. Lorenzi, S. Finkin, T. Hägglöf, A. Hurley, K. G. Millard, Y. Weisblum, F. Schmidt, T. Hatziioannou, P. D. Bieniasz, M. Caskey, D. F. Robbiani, M. C. Nussenzweig, P. J. Bjorkman, Structures of Human Antibodies Bound to SARS-CoV-2 Spike Reveal Common Epitopes and Recurrent Features of Antibodies. *Cell* **182**, 828–842.e16 (2020). doi:10.1016/j.cell.2020.06.025 Medline

18. L. L. Luchsinger, B. P. Ransegnola, D. K. Jin, F. Muecksch, Y. Weisblum, W. Bao, P. J. George, M. Rodriguez, N. Tricoche, F. Schmidt, C. Gao, S. Jawahar, M. Pal, E. Schnall, H. Zhang, D. Strauss, K. Yazdanbakhsh, C. D. Hillyer, P. D. Bieniasz, T. Hatziioannou, Serological Assays Estimate Highly Variable SARS-CoV-2 Neutralizing Antibody Activity in Recovered COVID-19 Patients. *J. Clin. Microbiol.* **58**, e02005-20 (2020). doi:10.1128/JCM.02005-20 Medline

19. F. Wu, M. Liu, A. Wang, L. Lu, Q. Wang, C. Gu, J. Chen, Y. Wu, S. Xia, Y. Ling, Y. Zhang, J. Xun, R. Zhang, Y. Xie, S. Jiang, T. Zhu, H. Lu, Y. Wen, J. Huang, Evaluating the Association of Clinical Characteristics With Neutralizing Antibody Levels in Patients Who Have Recovered From Mild COVID-19 in Shanghai, China. *JAMA Intern. Med.* **180**, 1356–1362 (2020). doi:10.1001/jamainternmed.2020.4616 Medline

20. B. J. DeKosky, T. Kojima, A. Rodin, W. Charab, G. C. Ippolito, A. D. Ellington, G. Georgiou, In-depth determination and analysis of the human paired heavy- and light-chain antibody repertoire. *Nat. Med.* **21**, 86–91 (2015). doi:10.1038/nm.3743 Medline

21. A. J. Greaney, A. N. Loes, K. H. D. Crawford, T. N. Starr, K. D. Malone, H. Y. Chu, J. D. Bloom, Comprehensive mapping of mutations in the SARS-CoV-2 receptor-binding domain that affect recognition by polyclonal human plasma antibodies. *Cell Host Microbe* **29**, 463–476.e6 (2021). doi:10.1016/j.chom.2021.02.003 Medline

22. T. F. Rogers, F. Zhao, D. Huang, N. Beutler, A. Burns, W. T. He, O. Limbo, C. Smith, G. Song, J. Woehl, L. Yang, R. K. Abbott, S. Callaghan, E. Garcia, J. Hurtado, M. Parren, L. Peng, S. Ramirez, J. Ricketts, M. J. Ricciardi, S. A. Rawlings, N. C. Wu, M. Yuan, D. M. Smith, D. Nemazee, J. R. Teijaro, J. E. Voss, I. A. Wilson, R. Andrabi, B. Briney, E. Landais, D. Sok, J. G. Jardine, D. R. Burton, Isolation of potent SARS-CoV-2 neutralizing antibodies and protection from disease in a small animal model. *Science* **369**, 956–963 (2020). doi:10.1126/science.abc7520 Medline

23. S. R. Leist, K. H. Dinnon 3rd, A. Schäfer, L. V. Tse, K. Okuda, Y. J. Hou, A. West, C. E. Edwards, W. Sanders, E. J. Fritch, K. L. Gully, T. Scobey, A. J. Brown, T. P. Sheahan,

N. J. Moorman, R. C. Boucher, L. E. Gralinski, S. A. Montgomery, R. S. Baric, A Mouse-Adapted SARS-CoV-2 Induces Acute Lung Injury and Mortality in Standard Laboratory Mice. *Cell* **183**, 1070–1085.e12 (2020). doi:10.1016/j.cell.2020.09.050 Medline

24. K. H. Dinnon 3rd, S. R. Leist, A. Schäfer, C. E. Edwards, D. R. Martinez, S. A. Montgomery, A. West, B. L. Yount Jr., Y. J. Hou, L. E. Adams, K. L. Gully, A. J. Brown, E. Huang, M. D. Bryant, I. C. Choong, J. S. Glenn, L. E. Gralinski, T. P. Sheahan, R. S. Baric, A mouse-adapted model of SARS-CoV-2 to test COVID-19 countermeasures. *Nature* **586**, 560–566 (2020). doi:10.1038/s41586-020-2708-8 Medline

25. D. Pinto, Y.-J. Park, M. Beltramello, A. C. Walls, M. A. Tortorici, S. Bianchi, S. Jaconi, K. Culap, F. Zatta, A. De Marco, A. Peter, B. Guarino, R. Spreafico, E. Cameroni, J. B. Case, R. E. Chen, C. Havenar-Daughton, G. Snell, A. Telenti, H. W. Virgin, A. Lanzavecchia, M. S. Diamond, K. Fink, D. Veesler, D. Corti, Cross-neutralization of SARS-CoV-2 by a human monoclonal SARS-CoV antibody. *Nature* **583**, 290–295 (2020). doi:10.1038/s41586-020-2349-y Medline

26. S. C. A. Nielsen, F. Yang, K. J. L. Jackson, R. A. Hoh, K. Röltgen, G. H. Jean, B. A. Stevens, J.-Y. Lee, A. Rustagi, A. J. Rogers, A. E. Powell, M. Hunter, J. Najeeb, A. R. Otrelo-Cardoso, K. E. Yost, B. Daniel, K. C. Nadeau, H. Y. Chang, A. T. Satpathy, T. S. Jardetzky, P. S. Kim, T. T. Wang, B. A. Pinsky, C. A. Blish, S. D. Boyd, Human B Cell Clonal Expansion and Convergent Antibody Responses to SARS-CoV-2. *Cell Host Microbe* **28**, 516–525.e5 (2020). doi:10.1016/j.chom.2020.09.002 Medline

27. S. D. Boyd, B. A. Gaëta, K. J. Jackson, A. Z. Fire, E. L. Marshall, J. D. Merker, J. M. Maniar, L. N. Zhang, B. Sahaf, C. D. Jones, B. B. Simen, B. Hanczaruk, K. D. Nguyen, K. C. Nadeau, M. Egholm, D. B. Miklos, J. L. Zehnder, A. M. Collins, Individual variation in the germline Ig gene repertoire inferred from variable region gene rearrangements. *J. Immunol.* **184**, 6986–6992 (2010). doi:10.4049/jimmunol.1000445 Medline

28. H. Tegally, E. Wilkinson, M. Giovanetti, A. Iranzadeh, V. Fonseca, J. Giandhari, D. Doolabh, S. Pillay, E. J. San, N. Msomi, K. Mlisana, A. von Gottberg, S. Walaza, M. Allam, A. Ismail, T. Mohale, A. J. Glass, S. Engelbrecht, G. Van Zyl, W. Preiser, F. Petruccione, A. Sigal, D. Hardie, G. Marais, N. Hsiao, S. Korsman, M.-A. Davies, L. Tyers, I. Mudau, D. York, C. Maslo, D. Goedhals, S. Abrahams, O. Laguda-Akingba, A. Alisoltani-Dehkordi, A. Godzik, C. K. Wibmer, B. T. Sewell, J. Lourenço, L. C. J. Alcantara, S. L. Kosakovsky Pond, S. Weaver, D. Martin, R. J. Lessells, J. N. Bhiman, C. Williamson, T. de Oliveira, Detection of a SARS-CoV-2 variant of concern in South Africa. *Nature* **592**, 438–443 (2021). doi:10.1038/s41586-021-03402-9

29. K. R. McCarthy, L. J. Rennick, S. Nambulli, L. R. Robinson-McCarthy, W. G. Bain, G. Haidar, W. P. Duprex, Recurrent deletions in the SARS-CoV-2 spike glycoprotein drive antibody escape. *Science* **371**, 1139–1142 (2021). doi:10.1126/science.abf6950 Medline

30. B. Choi, M. C. Choudhary, J. Regan, J. A. Sparks, R. F. Padera, X. Qiu, I. H. Solomon, H.-H. Kuo, J. Boucau, K. Bowman, U. D. Adhikari, M. L. Winkler, A. A. Mueller, T. Y.-T. Hsu, M. Desjardins, L. R. Baden, B. T. Chan, B. D. Walker, M. Lichterfeld, M. Brigl, D. S. Kwon, S. Kanjilal, E. T. Richardson, A. H. Jonsson, G. Alter, A. K. Barczak, W. P.

Hanage, X. G. Yu, G. D. Gaiha, M. S. Seaman, M. Cernadas, J. Z. Li, Persistence and Evolution of SARS-CoV-2 in an Immunocompromised Host. *N. Engl. J. Med.* **383**, 2291–2293 (2020). doi:10.1056/NEJMc2031364 Medline

31. V. A. Avanzato, M. J. Matson, S. N. Seifert, R. Pryce, B. N. Williamson, S. L. Anzick, K. Barbian, S. D. Judson, E. R. Fischer, C. Martens, T. A. Bowden, E. de Wit, F. X. Riedo, V. J. Munster, Case Study: Prolonged Infectious SARS-CoV-2 Shedding from an Asymptomatic Immunocompromised Individual with Cancer. *Cell* **183**, 1901–1912.e9 (2020). doi:10.1016/j.cell.2020.10.049 Medline

32. P. C. Resende *et al.*, The ongoing evolution of variants of concern and interest of SARS-CoV-2 in Brazil revealed by convergent indels in the amino (N)-terminal domain of the Spike protein. *medRxiv* 2021.03.19.21253946 [Preprint]. 20 March 2021. https://doi.org/10.1101/2021.03.19.21253946.

33. E. Andreano *et al.*, SARS-CoV-2 escape in vitro from a highly neutralizing COVID-19 convalescent plasma. *bioRxiv* 2020.12.28.424451 [Preprint]. 28 December 2020. https://doi.org/10.1101/2020.12.28.424451.

34. C. L. Hsieh, J. A. Goldsmith, J. M. Schaub, A. M. DiVenere, H.-C. Kuo, K. Javanmardi, K. C. Le, D. Wrapp, A. G. Lee, Y. Liu, C.-W. Chou, P. O. Byrne, C. K. Hjorth, N. V. Johnson, J. Ludes-Meyers, A. W. Nguyen, J. Park, N. Wang, D. Amengor, J. J. Lavinder, G. C. Ippolito, J. A. Maynard, I. J. Finkelstein, J. S. McLellan, Structure-based design of prefusion-stabilized SARS-CoV-2 spikes. *Science* **369**, 1501–1505 (2020). doi:10.1126/science.abd0826 Medline

35. R. Henderson, R. J. Edwards, K. Mansouri, K. Janowska, V. Stalls, S. M. C. Gobeil, M. Kopp, D. Li, R. Parks, A. L. Hsu, M. J. Borgnia, B. F. Haynes, P. Acharya, Controlling the SARS-CoV-2 spike glycoprotein conformation. *Nat. Struct. Mol. Biol.* **27**, 925–933 (2020). doi:10.1038/s41594-020-0479-4 Medline

36. E. Salazar, K. K. Perez, M. Ashraf, J. Chen, B. Castillo, P. A. Christensen, T. Eubank, D. W. Bernard, T. N. Eagar, S. W. Long, S. Subedi, R. J. Olsen, C. Leveque, M. R. Schwartz, M. Dey, C. Chavez-East, J. Rogers, A. Shehabeldin, D. Joseph, G. Williams, K. Thomas, F. Masud, C. Talley, K. G. Dlouhy, B. V. Lopez, C. Hampton, J. Lavinder, J. D. Gollihar, A. C. Maranhao, G. C. Ippolito, M. O. Saavedra, C. C. Cantu, P. Yerramilli, L. Pruitt, J. M. Musser, Treatment of Coronavirus Disease 2019 (COVID-19) Patients with Convalescent Plasma. *Am. J. Pathol.* **190**, 1680–1690 (2020). doi:10.1016/j.ajpath.2020.05.014 Medline

37. G. C. Ippolito, K. H. Hoi, S. T. Reddy, S. M. Carroll, X. Ge, T. Rogosch, M. Zemlin, L. D. Shultz, A. D. Ellington, C. L. Vandenberg, G. Georgiou, Antibody repertoires in humanized NOD-scid-IL2Rγ(null) mice and human B cells reveals human-like diversification and tolerance checkpoints in the mouse. *PLOS ONE* **7**, e35497 (2012). doi:10.1371/journal.pone.0035497 Medline

38. J. R. McDaniel, B. J. DeKosky, H. Tanno, A. D. Ellington, G. Georgiou, Ultra-high-throughput sequencing of the immune receptor repertoire from millions of lymphocytes. *Nat. Protoc.* **11**, 429–442 (2016). doi:10.1038/nprot.2016.024 Medline

39. A. M. Bolger, M. Lohse, B. Usadel, Trimmomatic: A flexible trimmer for Illumina sequence data. *Bioinformatics* **30**, 2114–2120 (2014). doi:10.1093/bioinformatics/btu170 Medline

40. D. A. Bolotin, S. Poslavsky, I. Mitrophanov, M. Shugay, I. Z. Mamedov, E. V. Putintseva, D. M. Chudakov, MiXCR: Software for comprehensive adaptive immunity profiling. *Nat. Methods* **12**, 380–381 (2015). doi:10.1038/nmeth.3364 Medline

41. R. C. Edgar, Search and clustering orders of magnitude faster than BLAST. *Bioinformatics* **26**, 2460–2461 (2010). doi:10.1093/bioinformatics/btq461 Medline

42. M. P. Lefranc, G. Lefranc, Immunoglobulins or Antibodies: IMGT® Bridging Genes, Structures and Functions. *Biomedicines* **8**, 319 (2020). doi:10.3390/biomedicines8090319 Medline

43. Y. H. Ching, T. K. Ghosh, S. J. Cross, E. A. Packham, L. Honeyman, S. Loughna, T. E. Robinson, A. M. Dearlove, G. Ribas, A. J. Bonser, N. R. Thomas, A. J. Scotter, L. S. D. Caves, G. P. Tyrrell, R. A. Newbury-Ecob, A. Munnich, D. Bonnet, J. D. Brook, Mutation in myosin heavy chain 6 causes atrial septal defect. *Nat. Genet.* **37**, 423–428 (2005). doi:10.1038/ng1526 Medline

44. K. Javanmardi *et al.*, Rapid characterization of spike variants via mammalian cell surface display. *bioRxiv* 2021.03.30.437622 [Preprint]. 30 March 2021. https://doi.org/10.1101/2021.03.30.437622.

45. Y. J. Hou, K. Okuda, C. E. Edwards, D. R. Martinez, T. Asakura, K. H. Dinnon 3rd, T. Kato, R. E. Lee, B. L. Yount, T. M. Mascenik, G. Chen, K. N. Olivier, A. Ghio, L. V. Tse, S. R. Leist, L. E. Gralinski, A. Schäfer, H. Dang, R. Gilmore, S. Nakano, L. Sun, M. L. Fulcher, A. Livraghi-Butrico, N. I. Nicely, M. Cameron, C. Cameron, D. J. Kelvin, A. de Silva, D. M. Margolis, A. Markmann, L. Bartelt, R. Zumwalt, F. J. Martinez, S. P. Salvatore, A. Borczuk, P. R. Tata, V. Sontake, A. Kimple, I. Jaspers, W. K. O'Neal, S. H. Randell, R. C. Boucher, R. S. Baric, SARS-CoV-2 Reverse Genetics Reveals a Variable Infection Gradient in the Respiratory Tract. *Cell* **182**, 429–446.e14 (2020). doi:10.1016/j.cell.2020.05.042 Medline

46. D. Tegunov, P. Cramer, Real-time cryo-electron microscopy data preprocessing with Warp. *Nat. Methods* **16**, 1146–1152 (2019). doi:10.1038/s41592-019-0580-y Medline

47. A. Punjani, J. L. Rubinstein, D. J. Fleet, M. A. Brubaker, cryoSPARC: Algorithms for rapid unsupervised cryo-EM structure determination. *Nat. Methods* **14**, 290–296 (2017). doi:10.1038/nmeth.4169 Medline

48. E. F. Pettersen, T. D. Goddard, C. C. Huang, E. C. Meng, G. S. Couch, T. I. Croll, J. H. Morris, T. E. Ferrin, UCSF ChimeraX: Structure visualization for researchers, educators, and developers. *Protein Sci.* **30**, 70–82 (2021). doi:10.1002/pro.3943 Medline

49. C. Michael, W. Mona, Y. Choonhan, *COSMIC2 – A Science Gateway for Cryo-Electron Microscopy* (2017).

50. J. Dunbar, K. Krawczyk, J. Leem, C. Marks, J. Nowak, C. Regep, G. Georges, S. Kelm, B. Popovic, C. M. Deane, SAbPred: A structure-based antibody prediction server. *Nucleic Acids Res.* **44** , W474–W478 (2016). doi:10.1093/nar/gkw361 Medline

51. E. F. Pettersen, T. D. Goddard, C. C. Huang, G. S. Couch, D. M. Greenblatt, E. C. Meng, T. E. Ferrin, UCSF Chimera—A visualization system for exploratory research and analysis. *J. Comput. Chem.* **25**, 1605–1612 (2004). doi:10.1002/jcc.20084 Medline

52. P. Emsley, K. Cowtan, Coot: Model-building tools for molecular graphics. *Acta Crystallogr. D Biol. Crystallogr.* **60**, 2126–2132 (2004). doi:10.1107/S0907444904019158 Medline

53. P. D. Adams, R. W. Grosse-Kunstleve, L.-W. Hung, T. R. Ioerger, A. J. McCoy, N. W. Moriarty, R. J. Read, J. C. Sacchettini, N. K. Sauter, T. C. Terwilliger, PHENIX: Building new software for automated crystallographic structure determination. *Acta Crystallogr. D Biol. Crystallogr.* **58**, 1948–1954 (2002). doi:10.1107/S0907444902016657 Medline

54. T. I. Croll, ISOLDE: A physically realistic environment for model building into low-resolution electron-density maps. *Acta Crystallogr. D Struct. Biol.* **74**, 519–530 (2018). doi:10.1107/S2059798318002425 Medline